INSTITUTE OF PHYSICS PUBLISHING JOURNAL OF PHYSICS B: ATOMIC, MOLECULAR AND OPTICAL PHYSICS

J. Phys. B: At. Mol. Opt. Phys. **35** (2002) 5141–5151 PII: S0953-4075(02)40148-4

Polarization spectroscopy of a closed atomic transition: applications to laser frequency locking

C P Pearman, C S Adams, S G Cox, P F Griffin, D A Smith and I G Hughes

Department of Physics, University of Durham, South Road, Durham DH1 3LE, UK

E-mail: i.g.hughes@durham.ac.uk

Received 23 July 2002, in final form 4 November 2002
Published 4 December 2002
Online at stacks.iop.org/JPhysB/35/5141

Abstract

We study polarization spectroscopy of Rb vapour. A weak probe beam analyses the birefringence induced in a room temperature vapour by a strong counterpropagating circularly polarized pump beam. In contrast to most other work on polarization spectroscopy, we use a polarization beam splitting cube and two detectors (rather than a polarizer and one detector) to analyse the probe beam. The signal is in the form of a derivative of a Lorentzian. For theoretical analysis we study the closed atomic transition $5\,^2S_{1/2}\,(F = 3) \rightarrow 5\,^2P_{3/2}\,(F' = 4)$ in the D2 line of ^{85}Rb. We study the time needed to redistribute population among the m_F states, derive an expression for the expected lineshape and present experimental data in excellent agreement with theory. The polarization spectrum provides an ideal error signal for frequency stabilization of a laser. We describe the geometry and parameters for optimizing the error signal.

1. Introduction

Polarization spectroscopy is an example of a sub-Doppler spectroscopic technique with counterpropagating pump and probe beams derived from the same laser [1–3]. The principle of polarization spectroscopy is to induce a birefringence in a medium, with a circularly polarized pump beam, and to interrogate this with a counterpropagating weak probe beam. It can be regarded as a form of saturation spectroscopy, with the change of the (complex) refractive index being proportional to the pump intensity, and as such is an example of a third-order nonlinear effect [4]. Polarization spectroscopy in molecules is a useful technique for combustion diagnostics, and is reviewed in this context in [5].

Most work on polarization spectroscopy has used a single detector, passing the probe beam through (nearly) crossed polarizers [3]. In this work, we use two detectors, and a polarization beam splitting cube, similar to the scheme employed by Hänsch and Couillaud for stabilization of a laser frequency to a reflecting reference cavity [6]. In addition we study Rb vapour, which

provides an easily saturable medium where one can neglect collisions and use a laser with a linewidth less than the natural width of the transition. This is a rather different environment to that studied in combustion diagnostics, where collisional relaxation in ground and excited states, quenching, the finite laser linewidth and its multi-axial mode structure are important [7].

For closed transitions, we demonstrate that the polarization spectrum has a derivative lineshape, which is ideal as a signal for actively stabilizing the laser frequency. The frequency spectrum of the laser can be 'locked' to the atomic spectrum, with a width narrower than that of the natural linewidth. Such ultra-stable lasers have many applications, ranging from precision measurements to optical communications and laser cooling of atoms and ions. There has been an explosion of interest in the field of laser cooling in recent years [8], where cold atoms can be manipulated by light forces [9] and magnetic fields [10].

In the next section we obtain expressions for the polarization signal, and outline the benefits of the method described in this paper. In section 3 we develop a technique for calculating the anisotropy of the medium; section 4 contains the experimental results; in section 5 we discuss issues relating to using the polarization signal for frequency stabilization of the laser and we draw our conclusions in section 6.

2. Theory

It is desirable to obtain a polarization signal which has zero background. The conventional way to achieve this is to use crossed polarizers in the probe beam, one before and one after the cell containing the medium to be analysed. The probe does not transmit through to a photodetector behind the second polarizer in the absence of the pump. The presence of the pump causes the plane of polarization of the probe to be rotated through a small angle, Φ (calculated below). Malus's law can then be used to predict a transmitted intensity of $I = I_0 \sin^2 \Phi \sim I_0 \Phi^2$. The method we employ here involves having the plane of polarization of the probe beam at $\pi/4$ with respect to an analyser (a polarizing beam splitter). In the absence of the pump the intensity in one arm of the polarizing beam splitter ($I_x = I_0 \cos^2 \pi/4 = I_0/2$) is equal to the intensity in the other arm ($I_y = I_0 \sin^2 \pi/4 = I_0/2$). Subtracting these gives a zero signal in the absence of the pump. When the pump is present, a rotation through a small angle, Φ, of the plane of polarization of the probe leads to a difference of signals $I_y - I_x = 2I_0\Phi$. Therefore, we expect a signal that is larger with the set-up used in this work compared to the conventional technique. We now derive expressions for the amplitude and shapes of the polarization signals obtained with the two methods.

The direction of propagation of the probe beam defines the z axis. We write the initial state, which is linearly polarized in a plane at an angle φ with respect to the x axis, as

$$\boldsymbol{E} = \begin{bmatrix} E_x \\ E_y \end{bmatrix} = E_0 \begin{bmatrix} \cos\varphi \\ \sin\varphi \end{bmatrix}. \tag{1}$$

It is also convenient to rewrite this in terms of the circular polarization basis vectors,

$$\boldsymbol{E} = E_0 \begin{bmatrix} \cos\varphi \\ \sin\varphi \end{bmatrix} = E_0 \left\{ \frac{\mathrm{e}^{-\mathrm{i}\varphi}}{2} \begin{bmatrix} 1 \\ \mathrm{i} \end{bmatrix} + \frac{\mathrm{e}^{\mathrm{i}\varphi}}{2} \begin{bmatrix} 1 \\ -\mathrm{i} \end{bmatrix} \right\}. \tag{2}$$

In propagating through the cell of length L, the beam's components experience differential absorption and dispersion on account of the gas and cell windows. The birefringence in the cell windows is caused by the pressure gradient across them and the manufacture process. The electric field of the probe beam after the cell is thus

$$\boldsymbol{E} = E_0 \left\{ \frac{\mathrm{e}^{-\mathrm{i}\varphi}}{2} \begin{bmatrix} 1 \\ \mathrm{i} \end{bmatrix} \mathrm{e}^{-\mathrm{i}k_+ L} \mathrm{e}^{-\alpha_+ L/2} \mathrm{e}^{-\mathrm{i}k_{w+} l} + \frac{\mathrm{e}^{\mathrm{i}\varphi}}{2} \begin{bmatrix} 1 \\ -\mathrm{i} \end{bmatrix} \mathrm{e}^{-\mathrm{i}k_- L} \mathrm{e}^{-\alpha_- L/2} \mathrm{e}^{-\mathrm{i}k_{w-} l} \right\}. \tag{3}$$

Here $k_\pm = \frac{\omega}{c} n_\pm$; $n_\pm$ are the refractive indices of the gas for the circular polarization components which drive $\sigma^\pm$ transitions; $\alpha_\pm$ are the corresponding absorption coefficients and the $k_{w\pm} = \frac{\omega}{c} n_{w\pm}$ terms describe the phase change picked up traversing the window of width l. The refractive indices of the windows can be complex; therefore, we write them as [3] $n_{w\pm} l = b_{R\pm} - \mathrm{i}\frac{c}{\omega} b_{I\pm}$. We can rewrite this expression as

$$\boldsymbol{E} = E_0 \exp\left\{-\mathrm{i}\left[\frac{\omega}{c}(nL + b_R) - \mathrm{i}b_I - \mathrm{i}\frac{\alpha L}{2}\right]\right\}\left\{\frac{\mathrm{e}^{-\mathrm{i}\varphi}}{2}\begin{bmatrix}1\\ \mathrm{i}\end{bmatrix}\mathrm{e}^{+\mathrm{i}\Omega} + \frac{\mathrm{e}^{\mathrm{i}\varphi}}{2}\begin{bmatrix}1\\ -\mathrm{i}\end{bmatrix}\mathrm{e}^{-\mathrm{i}\Omega}\right\}. \tag{4}$$

Here,

$$\Omega = \frac{\omega}{2c}(\Delta n L + \Delta b_R) - \mathrm{i}\left(\frac{L}{4}\Delta\alpha + \frac{1}{2}\Delta b_I\right), \tag{5}$$

and

$$\begin{aligned} &n = \tfrac{1}{2}(n_+ + n_-), \quad \alpha = \tfrac{1}{2}(\alpha_+ + \alpha_-), \quad b_R = \tfrac{1}{2}(b_{R+} + b_{R-}), \quad b_I = \tfrac{1}{2}(b_{I+} + b_{I-}) \\ &\Delta n = n_+ - n_-, \quad \Delta\alpha = \alpha_+ - \alpha_-, \quad \Delta b_R = b_{R+} - b_{R-}, \quad \Delta b_I = b_{I+} - b_{I-}. \end{aligned} \tag{6}$$

The probe beam is decomposed into horizontal (x) and vertical (y) components by the beam splitting cube, and the difference in intensity ($I \propto |E|^2$) of the two components gives the polarization spectroscopy signal:

$$\begin{aligned} I_{signal} &= I_y - I_x \\ I_{signal} &= I_0 \mathrm{e}^{-\alpha L - 2b_I} \cos\left(2\varphi + L\Delta n\frac{\omega}{c} + \Delta b_R \frac{\omega}{c}\right) \end{aligned} \tag{7}$$

with I_0 the intensity of the probe beam in the absence of the cell. So far, the analysis has been exact. We now make approximations that simplify these results. The birefringence in the cell is typically very small, and the rotation angle induced by the anisotropic medium, $\Phi = \frac{2\pi(n_+ - n_-)}{\lambda} L$, is also very small. We assume that the laser frequency is scanned across a single resonance (this is justified in section 3). The spectral profile of the difference in absorption is a (power broadened) Lorentzian,

$$\Delta\alpha = \frac{\Delta\alpha_0}{1 + x^2}, \tag{8}$$

where $\Delta\alpha_0$ is the maximum difference in absorption at the line centre, and $x = \frac{\omega_0 - \omega}{\Gamma/2}$ is the scaled detuning in units of half the (power broadened) linewidth, Γ. Accompanying the modification in absorption coefficient is a concomitant change to the refractive index of the medium. The absorption coefficient and the refractive index are related by the Kramers–Kronig dispersion relation [3], $\Delta n = \frac{c}{\omega_0}\Delta\alpha_0 \frac{x}{1+x^2}$. For the typical case of the angular rotation induced by the medium being small, the signal in equation (7) is maximized when $\varphi = \frac{\pi}{4}$. In this approximation the signal is

$$I_{signal} = -I_0 \mathrm{e}^{-\alpha L - 2b_I}\left(L\Delta\alpha_0 \frac{x}{1 + x^2} + \Delta b_R \frac{\omega}{c}\right), \tag{9}$$

i.e. we obtain a signal that is dispersion shaped, being the derivative of the sub-Doppler linewidth. This remains true for a wide range of angles, centred around $\varphi = \frac{\pi}{4}$, at which the maximum amplitude is obtained. This technique yields a dispersion shaped curve on a zero background, which is ideal for frequency stabilization of the laser by 'locking' to the polarization spectrum (see section 5). For the case of φ being small or close to $\pi/2$, corresponding to the probe beam being nearly aligned with one of the axes of the beam

splitting cube, the signal is of the form $1 - \frac{1}{2}(L\Delta\alpha_0 \frac{x}{1+x^2})^2$. Under these conditions, the signal is similar to a conventional absorption line in a broader dip, with a much smaller amplitude[1].

It is interesting to compare the size and shape of the signal obtained here with that resulting from the conventional experimental set-up with one detector. In that case, the analyser is a linear polarizer slightly misaligned from the vertical. The probe beam is horizontally polarized and a change in signal is detected when the plane of polarization of the probe is rotated. If ϑ is the misalignment angle of the polarizer relative to the vertical axis, the transmitted electric field is

$$E_t = E_x \sin(\vartheta) + E_y \cos(\vartheta). \tag{10}$$

The transmitted intensity is easily calculated, and simplifies in the case where the medium induces a small angular rotation, see for example equation (7.41) of [3]. With this configuration, there is a derivative contribution to the lineshape and a Lorentzian. The relative contribution of each term depends on the anisotropy of the medium, the birefringence in the cell windows and the misalignment angle. The coefficient of the derivative term is smaller in this expression than in equation (9) by a factor of ϑ', where $\vartheta' = \vartheta + \Delta b_r \frac{\omega}{2c}$. We will show in section 4 that this makes the signal obtained with the method outlined in this work an order of magnitude larger.

3. The magnitude of the anisotropy of the medium

We have shown that the anisotropy of the medium can be represented by one parameter, the differential line-centre absorption. We now turn our attention to studying how this depends on the pump laser. The key issue is whether the complex interaction of a multi-level atom with the pump beam allows a significant build-up of anisotropy in the time an atom traverses the laser beam (the transit time).

The two-level atom model is insufficient to explain the hyperfine-resolved spectra of alkali metal atoms on the D2 transition. For an atom with nuclear spin I, there are two values of the angular momentum for the ground state ($F = I \pm 1/2$), and four for the excited state ($F' = I \pm 3/2,\ I \pm 1/2$). There are two transitions which dominate in polarization spectroscopy, $F = I + 1/2 \rightarrow F' = I + 3/2$ and $F = I - 1/2 \rightarrow F' = I - 3/2$. This is because these transitions are closed, i.e. the electric dipole selection rule ($\Delta F = 0,\ \pm 1$) prevents atoms from falling into the other ground state. For example, in ^{85}Rb ($I = 5/2$) the transitions $F = 3 \rightarrow F' = 2$ or 3 have a decay channel to the $F = 2$ hyperfine level in the ground state. Atoms in this level are very far from resonance ($\sim$3 GHz) with the probe, consequently they do not cause a rotation in the plane of polarization of the probe. As a result, we expect the polarization spectroscopy signal to be greatly enhanced on the $F = 3 \rightarrow F' = 4$ transition compared with $F = 3 \rightarrow F' = 2$ or 3. For transitions from the other hyperfine ground state, we expect $F = 2 \rightarrow F' = 1$ to produce the largest polarization signal.

As the atoms start with a uniform distribution among the m_F states, they need to absorb a finite number of pump photons to redistribute the population asymmetrically. In order to see how large a signal one might expect, we studied the number of photons per atom needed to optically pump the population towards the equilibrium state. The calculations were performed for the $F = 3 \rightarrow F' = 4$ transition, for which the equilibrium state is $F = 3, m_F = 3$. Figure 1 shows the relative line-strength factors. A quantity of interest is the average number of photons needed to transfer a given initial m_F state into the equilibrium state. This was

[1] Note that the sum of the intensities from the photodiodes gives a signal which is independent of the angle of polarization of the probe beam, and corresponds to the absorption spectrum obtained in conventional pump–probe spectroscopy without polarization analysis. This gives a convenient method of obtaining a reference spectrum to locate the polarization features.

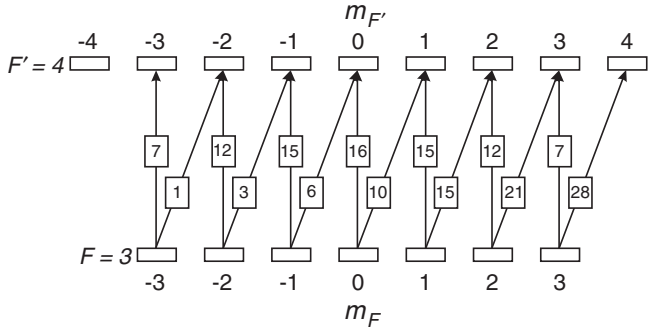

Figure 1. The relative strengths of σ^+ and π transitions in the $F = 3 \rightarrow F' = 4$ line in ^{85}Rb. The strengths of σ^- transitions are obtained from the reflection of the σ^+ transitions, i.e. $(3, -3)$ to $(4, -4)$ has the same strength as $(3, 3)$ to $(4, 4)$. The weakest transition has been scaled to be 1.

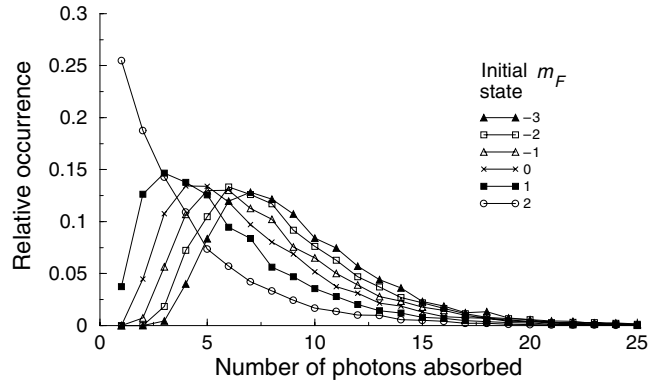

Figure 2. The distribution of the number of photons needed to transfer atoms into the extreme state, for different initial m_F states. The Monte Carlo simulation had 10 000 atoms in each initial state and used the line-strength factors of figure 1.

calculated by running a Monte Carlo simulation for 10 000 atoms in each initial state. Each atom undergoes the transition $F = 3, m_F \rightarrow F' = 4, m_{F'} = m_F + 1$ on absorbing a pump photon; the emission can be any one of the three $F' = 4, m_{F'} \rightarrow F = 3, m_F = m_{F'} \pm 1, m_{F'}$. The probability of each spontaneous transition is calculated from the line-strength factors of figure 1. The pressure in the cell is sufficiently low ($\sim 10^{-7}$ mbar) that we can disregard the effect of collisional redistribution of population in the excited state. The distribution of the number of photons needed to transfer atoms into the extreme state, for different initial states, is shown in figure 2. It is possible to calculate the average values analytically using Markov chain analysis with the Chapman–Kolmogorov equations [11]. The comparison between this method and the Monte Carlo method is summarized in table 1.

By combining the photon transfer distribution with the line-strength factors (optical pumping times), we can model the time dependence of the anisotropy. As the line strength factors vary by more than an order of magnitude, atoms in states with negative m_F values will take much longer to undergo a σ^+ transition. As a typical thermal speed for atoms in the vapour is 300 m s^{-1}, and the laser beams used in our experiments have widths of order 1 mm, the typical transit time is a few microseconds. We therefore studied the evolution of the anisotropy of the atoms on this timescale. Figure 3 shows the growth of anisotropy as a function of time,

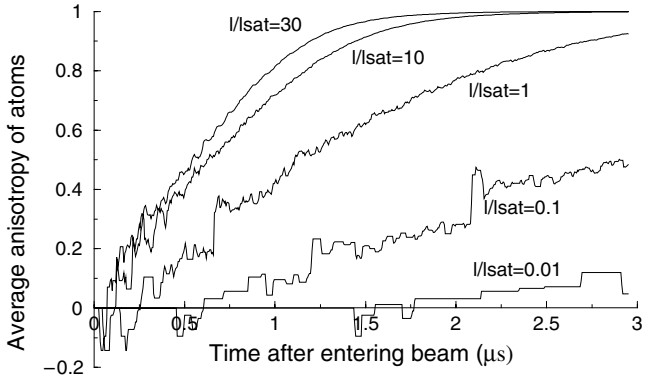

Figure 3. The growth of anisotropy as a function of time, for different pump laser intensities. For a thermal speed of 300 m s^{-1} and a beam width of 1 mm, the average time spent in the beam is 3 μs.

Table 1. The average and standard deviation for the number of photons needed for an atom in a given initial m_F state to be optically pumped into the equilibrium state. The average is calculated both by a Monte Carlo method and using Markov chains; the standard deviation is obtained from the Monte Carlo simulation.

m_F	−3	−2	−1	0	1	2
Average	9.4	8.8	8.0	7.1	5.8	4.0
Standard deviation	4.0	4.0	4.0	4.0	3.8	3.5

for different values of pump intensity. The 'trajectories' of 10 000 atoms for a given m_F state ($-3 \leqslant m_F \leqslant 2$) were followed, for different values of pump intensity. The initial distribution among m_F states was uniform. The time at which each atom absorbs a photon is recorded, taking into account the intensity dependence of the optical pumping rate. Subsequently, the atom falls into a particular m_F state with probability determined by the relevant line strength factors for spontaneous emission. The anisotropy for a given m_F state is the difference in absorption coefficients for σ^+ and σ^- transitions. The ensemble anisotropy is scaled in terms of units of the maximum anisotropy, when all atoms are pumped into $F = 3, m_F = 3$. Figure 3 shows that for an intensity similar to the saturation intensity (easily exceeded in the case of Rb vapour with diode lasers) a large anisotropy is established within the transit time.

4. Experimental results

The layout of the experiment is shown in figure 4. Both pump and probe are derived from the same extended cavity diode laser (ECDL). The laser has a Sanyo DL-7140-201 chip, collimated with a 4.5 mm focal length, aspheric lens, to give an output beam with spot radii ($1/e^2$ intensity) of 0.7 mm vertically and 1.4 mm horizontally. The counterpropagating pump and probe beams overlap with a crossing angle of 12 mrad in a 50 mm long vapour cell, containing ^{85}Rb and ^{87}Rb, in their natural abundances at room temperature. Neutral density filters are used to vary the pump and probe powers independently. A half-wave plate is used to rotate the plane of polarization of the probe beam with respect to the axis of the beam splitting cube; a quarter-wave plate is used to convert the pump to have circular polarization. The two output beams from the beam splitting cube are focused onto photodiode circuits, which record a voltage linearly proportional to the incident intensity. Typically, only a small fraction of light

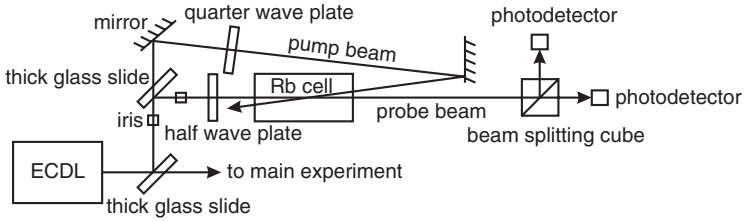

Figure 4. The experimental layout. A thick glass slide picks off a fraction of light fed from the ECDL, and a second glass slide picks off the probe beam. The (nearly) counterpropagating pump and probe beams overlap in a 50 mm long Rb vapour cell. A half-wave plate is used to rotate the plane of polarization of the probe beam with respect to the axis of the beam splitting cube; a quarter-wave plate is used to make the pump circularly polarized.

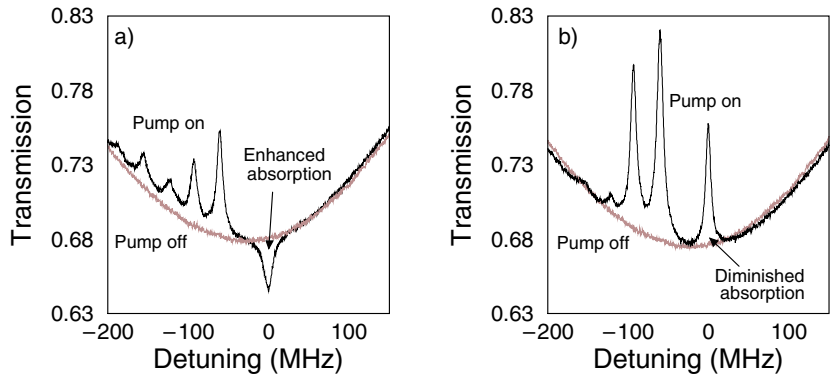

Figure 5. Spectra obtained with a quarter-wave plate inserted before the beam splitting cube. (a) Absorption profile for the component of the probe driving σ^+ transitions, showing an enhanced absorption in the region of the closed transition. (b) Absorption profile for the component of the probe driving σ^- transitions, showing diminished absorption in the region of the closed transition. The pump-off trace is shown in grey.

is fed into the polarization spectrometer (up to a few milliwatts); the rest can be used for an auxiliary experiment.

Our first experiment was to verify the conclusion of the last section, that an observable anisotropy could be induced in a typical transit time. A quarter-wave plate was inserted before the beam splitting cube, oriented such that it converted the circular polarization component of the probe which drives $\sigma^+(\sigma^-)$ transitions into vertically (horizontally) polarized light. The output from the arms of the analyser then directly measures the absorption experienced by the components driving σ^+ and σ^- transitions. Figure 5 shows the data obtained. Each figure has two traces, corresponding to the pump off and on respectively. With no pump, we obtain the conventional Doppler broadened absorption spectrum. With the pump present, we see a significant modification of the absorption spectrum at some frequencies. This can be mostly attributed to hyperfine pumping into the $F = 2$ ground state. However, in the vicinity of the $F = 3 \rightarrow F' = 4$ transition we expect the absorption to be modified on account of the anisotropy induced by the circularly polarized pump beam. Figure 5(a) displays the absorption profile for the component of the probe driving σ^+ transitions, showing an enhanced absorption in the region of the closed transition, whereas, in contrast, the absorption of the component of the probe driving σ^- transitions is reduced in figure 5(b). This demonstrates that an anisotropy is established.

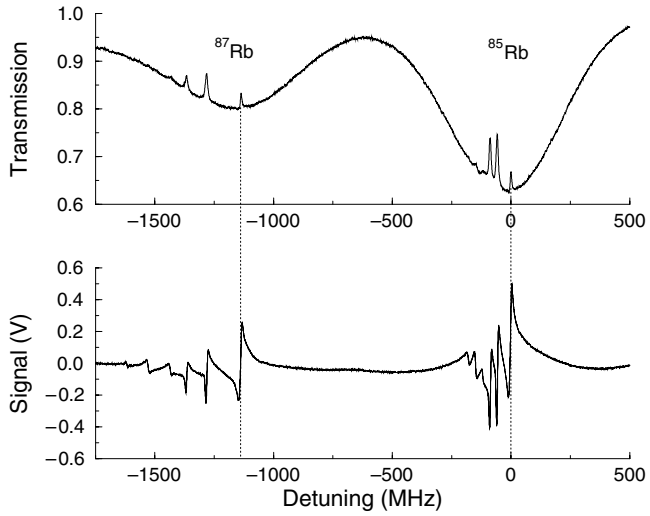

Figure 6. Typical experimental results obtained with a weak probe beam (power $\sim 1\ \mu$W). The upper trace shows the absorption spectrum for the transitions $F = 2 \rightarrow F' = 3, 2, 1$ in ^{87}Rb (left) and for $F = 3 \rightarrow F' = 4, 3, 2$ in ^{85}Rb (right). The lower trace is the polarization spectrum. Each absorption line in the upper trace has a corresponding dispersive feature. The strongest polarization features arise from the closed transitions $F \rightarrow F' = F + 1$.

An important issue in pump–probe spectroscopy relates to the power used for the probe beam. Typically, one studies the modification of the spectra obtained for a range of pump powers for a given probe power. However, the spectra obtained also depend strongly on the probe power. This is due to the presence of two hyperfine ground states. Transitions of the form $F = I + 1/2 \rightarrow F' = I + 1/2, I - 1/2$ have electric dipole allowed transitions to the other ground state, $F = I - 1/2$. This hyperfine pumping depletes the number of atoms in the upper hyperfine ground state, which diminishes the absorption. The probe beam does not have to be large compared with the saturation intensity for this effect to be important. Provided the hyperfine pumping time is comparable to the transit time this mechanism will be significant. For example, for the transitions $F = 3 \rightarrow F' = 4, 3, 2$ in ^{85}Rb, the line-centre transmission increases monotonically from 66% for probe powers less than 1 μW to 87% for 200 μW.

Typical experimental results obtained with a weak probe ($\leqslant 1\ \mu$W) are shown in figure 6. The data were taken with a pump power of 10 μW, and a probe power of 1 μW. The upper trace plots the transmission through the cell as a function of laser frequency. Zero detuning is relative to the $F = 3 \rightarrow F' = 4$ transition in ^{85}Rb. The saturated absorption/hyperfine pumping spectrum [3] for the transitions $F = 3 \rightarrow F' = 4, 3, 2$ in ^{85}Rb, and $F = 2 \rightarrow F' = 3, 2, 1$ in ^{87}Rb are seen. The lower trace shows the polarization spectrum. Conventional 'saturated absorption' spectra have six peaks—three features when the laser is resonant with transitions $F \rightarrow F' = F \pm 1, F$; and three cross over features when the laser is tuned halfway between two resonances. In ^{85}Rb, for transitions from the upper hyperfine ground state, only $F = 3 \rightarrow F' = 4$ gives a genuine saturated absorption feature; all other transitions have a decay mechanism into the $F = 2$ ground state. This hyperfine pumping depletes atoms that would have absorbed the probe; consequently, there is an increase in transmission. Similarly, from the upper hyperfine ground state in ^{87}Rb, only $F = 2 \rightarrow F' = 3$ gives a genuine saturated absorption feature. However, as predicted in section 3, the polarization signals for the closed transitions $F = 3 \rightarrow F' = 4$ in ^{85}Rb and $F = 2 \rightarrow F' = 3$ in ^{87}Rb are expected to be the largest—this is seen clearly in the figure. To obtain a signal for frequency stabilization

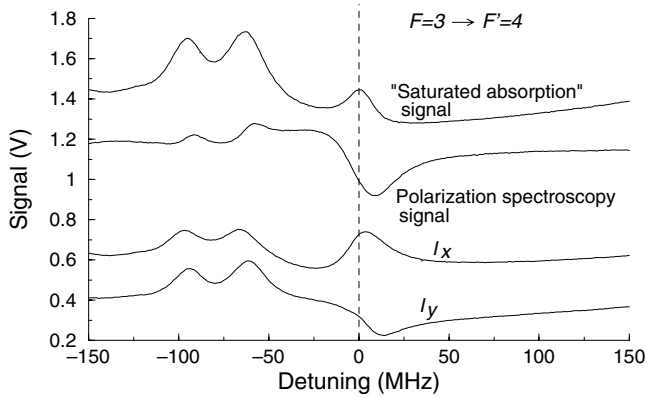

Figure 7. Polarization spectroscopy with pump and probe powers 1.2 and 0.12 mW respectively. The two bottom traces correspond to the signals from the separate arms of the beam splitting cube (I_x and I_y); the trace above these is the difference between them (the polarization spectroscopy signal); the top trace is the sum of the bottom two (conventional 'saturated absorption' and hyperfine pumping spectroscopy). The traces are offset vertically, for clarity.

of the laser, it is desirable for the derivative of the closed transitions to dominate. This is achieved by increasing the power in both the pump and probe beams.

Figure 7 shows typical experimental results outside the weak-probe regime. These traces were taken with a probe power of 120 μW and a pump power of 1.2 mW. The two bottom traces correspond to the signals from the separate arms of the beam splitting cube (I_x and I_y); the difference between these gives the polarization spectroscopy signal; the upper trace is their sum (conventional saturated absorption/hyperfine pumping spectroscopy). The traces are offset vertically, for clarity. Zero detuning in this figure is relative to the $F = 3 \rightarrow F' = 4$ line centre. Under these conditions, the polarization spectrum is dominated by the contribution from the $F = 3 \rightarrow F' = 4$ resonance. This spectrum is ideal for locking the laser: note especially the absence of other zero crossings in the signal, in contrast to figure 6.

Figure 8 shows a comparison between the experimental and theoretical line shapes. Figure 8(a) shows the signal obtained for the probe polarization oriented at $\varphi = \pi/4$. The thick curve is a fit (the parameters $\Delta\alpha_0$, a frequency offset and a vertical scaling were allowed to float) to the form of equation (7). Experiment and theory show excellent agreement. (The small ripples in the experimental signal at the extreme red detuning arise from the presence of the other transitions.) The data are consistent with no significant cell window birefringence. Figure 8(b) shows data obtained under the same conditions, with a rotation of the plane of polarization of the probe to be $\varphi = \pi/6$. The parameters for the theoretical prediction are identical to figure 8(a), apart from changing φ and allowing an offset. The signal is still a derivative line shape, but with reduced amplitude. There is excellent agreement between the reduction in amplitude predicted by our theory and that seen experimentally. We also compared the magnitude of the signals obtained with the method outlined here and those obtained with the conventional technique. The peak-to-peak signal we obtain is 20 times larger than that obtained with a single detector and an offset angle of $\vartheta = 5°$.

Lifting the degeneracy of the different m_F ground states by applying an external magnetic field changes the polarization spectrum. Three pairs of coils along orthogonal Cartesian axes around the cell were used to change the magnetic field. Experimentally, we find an optimal signal when we completely cancel the earth's field (optimal here meaning the largest signal with the steepest slope through zero). We find a decrease in the peak-to-peak value of the signal by a factor of two if the earth's field is not cancelled. Adding additional fields in other

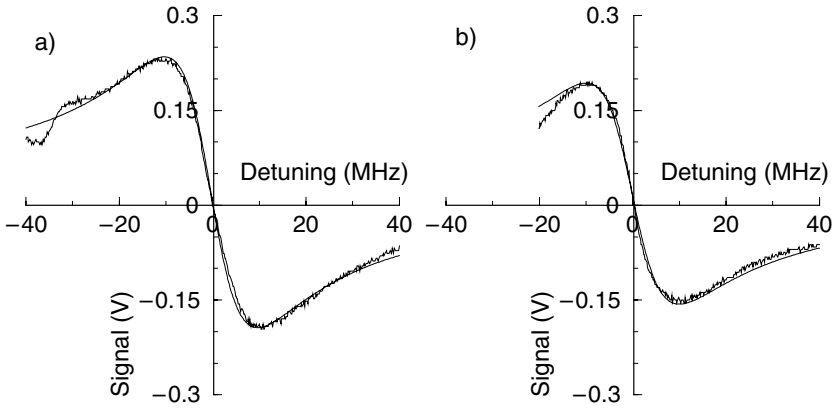

Figure 8. (a) Signal obtained for $\varphi = \pi/4$. The thick line is a fit to the form of equation (7). The thin curve is the experimental data. Experiment and theory show excellent agreement. The anisotropy of the medium, the line centre and a vertical scaling were allowed to float in the fit. (b) Data obtained under the same conditions, with a rotation of the plane of polarization of the pump to be $\varphi = \pi/6$. The parameters for the theoretical prediction are identical to the main figure, apart from changing φ and allowing an offset.

directions only served to reduce the signal. For large applied fields, the polarization spectrum is severely distorted as the degeneracy of the Zeeman levels is lifted.

5. Laser frequency stabilization

The polarization signal of figure 7 is ideal for locking the laser. (Polarization spectroscopy has already been used to stabilize the frequency of a diode laser for laser-cooling experiments [12].) We built a feedback circuit taking the polarization signal as the input. Typically, we chose the gain of the photodiode circuits such that we recorded an absorption signal of the order of a volt; under these circumstances we obtained a polarization signal of a few hundred millivolts. We did not amplify this signal further. The polarization spectroscopy signal was fed into an integrator and the output fed through a low-pass filter, used as the feedback to the piezo-electric transducer controlling the length of the external cavity of the laser. The laser locked tightly to the polarization spectrum, and was very resilient against typical mechanical perturbations found in a laboratory. The capture range is very broad, the nearest zero crossing in the polarization spectrum being GHz away. Based on the polarization signal, we estimated the locked linewidth of the laser to be 300 kHz for a 500 ms observation time. A higher stability might be obtained by feeding back the high-frequency component of the feedback signal to the laser current [13].

The location of the zero crossing relative to the centre of the $F = 3 \rightarrow F' = 4$ transition is dependent on the pump power, a factor which has to be taken into account. There are other effects which lead to a slow drift of the zero crossing (quite a few of the optical components used have temperature-dependent birefringence properties). The polarization spectrum is ideal for locking to the centre of the closed transition $F = 3 \rightarrow F' = 4$. However, in laser-cooling experiments, typically one wants to lock the laser to a frequency detuned a few linewidths to the red of the transition for most effective cooling [9]. We achieve this by placing an acousto-optic modulator in the polarization spectrometer and another in the main beam for the experiment. This allows us to tune the laser frequency used in the main experiment with respect to the centre of the transition. It is also possible to offset lock the laser to a frequency different to

that of the zero crossing of the polarization spectrum[2]. For transitions from the lower ground state, the zero-crossing polarization spectrum obtained can be used, when offset, to lock the 'repumping' laser to obtain a magneto-optical trap.

6. Conclusions

In this paper we have analysed theoretically a set-up for polarization spectroscopy using an analyser and two detectors. This gives a dispersion lineshape which is significantly larger than that obtained by the conventional single-detector approach. We modelled the evolution of the anisotropy of the medium as a function of the atom–light interaction time, taking into account the multi-level atomic structure and the different line strength factors. We showed that a pump intensity of the order of the saturation intensity is sufficient to generate a significant anisotropy. The presence of this anisotropy was demonstrated by observing the different absorption spectra obtained with the left and right hand circularly polarized components of a probe beam. We demonstrated that the lineshape of the polarization spectra is dependent on the probe power. Outside the weak-probe regime we obtain spectra that are dominated by a single hyperfine transition, which are ideal for frequency stabilization of the laser. Compared to dither locking of a saturated absorption feature, the standard method used for frequency stabilization of the laser, the method described here has the advantages of not needing a lock-in amplifier; having a larger capture range and eliminating frequency modulation of the laser. The disadvantage of this method is that the zero crossing does not necessarily coincide with the exact line position. However, as adding the signals from the two photodiodes gives a reference saturated absorption signal, it is easy to locate the zero crossing relative to the line centre.

Acknowledgments

We are grateful to Wing Ng for help with constructing the experiment; for expert technical assistance and loan of equipment from Wayne Dobby and Ian Manfren and for valuable discussions with Aidan Arnold and Ben Sauer. This work was supported by EPSRC and Durham University.

References

[1] Wieman C and Hänsch T W 1976 *Phys. Rev. Lett.* **36** 1170
[2] Teets R E, Kowalski F V, Hill W T, Carlson N and Hänsch T W 1977 Advances in laser spectroscopy *SPIE* **113** 80
[3] Demtröder W 1998 *Laser Spectroscopy* 2nd edn (Berlin: Springer)
[4] Levenson M D and Kano S S 1988 *Introduction to Nonlinear Laser Spectroscopy* (San Diego, CA: Academic)
[5] Eckbreth A C 1996 *Laser Diagnostics for Combustion Temperature and Species* (Amsterdam: Overseas Publishers Association)
[6] Hänsch T W and Couillaud B 1980 *Opt. Commun.* **35** 441
[7] Walewski J, Kaminski C F, Hanna S F and Lucht R P 2001 *Phys. Rev.* A **64** 063816
[8] Chu S 1998 *Rev. Mod. Phys.* **70** 685
Cohen-Tannoudji C N 1998 *Rev. Mod. Phys.* **70** 707
Phillips W D 1998 *Rev. Mod. Phys.* **70** 721
[9] Adams C S and Riis E 1997 *Prog. Quantum Electron.* **21** 1
Metcalf H J and van der Straten P 1999 *Laser Cooling and Trapping* (Berlin: Springer)
[10] Hinds E A and Hughes I G 1999 *J. Phys. D: Appl. Phys.* **32** R119
[11] Pearman C 2002 Ultra stable lasers for atom cooling *MSci Report* Durham University
[12] Lancaster G P T, Conroy R S, Clifford M A, Arlt J and Dholakia K 1999 *Opt. Commun.* **170** 79
[13] Rovera G D, Santarelli G and Clairon A 1994 *Rev. Sci. Instrum.* **65** 1502

[2] Such a scheme is used successfully in laser cooling experiments at Sussex University (E Hinds and C Vale, private communication).